Ion-induced soot nucleation using a new potential for curved aromatics

Kimberly Bowal[1], Jacob W. Martin[1,2], Alston J. Misquitta[3], Markus Kraft[1,2,4]

[1]Department of Chemical Engineering and Biotechnology, University of Cambridge,
West Site, Philippa Fawcett Drive, Cambridge CB3 0AS, UK

[2]Cambridge Centre for Advanced Research and Education in Singapore (CARES)
CREATE Tower, 1 Create Way, Singapore, 138602

[3]School of Physics and Astronomy, and the Thomas Young Centre for Theory and Simulation of Materials, Queen Mary University of London
327 Mile End Road, London E1 4NS, UK

[4]School of Chemical and Biomedical Engineering, Nanyang Technological University
62 Nanyang Drive, Singapore, 637459

submitted to *Combustion Science and Technology*

December 10, 2018

short running title: Soot nucleation using a new potential for curved aromatics

keywords: force field, curved polycyclic aromatic hydrocarbon, flexoelectric dipole, ion-induced nucleation, soot formation

[2]Corresponding Author: e-mail: mk306@cam.ac.uk

Abstract

A potential able to capture the properties and interactions of curved polycyclic aromatic hydrocarbons (cPAHs) was developed and used to investigate the nucleation behaviour and structure of nascent soot particles. The flexoelectric charge polarisation of cPAHs caused by pentagon integration was included through the introduction of off-site virtual atoms, and enhanced dispersion interaction parameters were fitted. The electric polarisation and intermolecular interactions of cPAHs were accurately reproduced compared to *ab initio* calculations. This potential was used within molecular dynamics simulations to examine the homogeneous and heterogeneous nucleation behaviour of the cPAH corannulene and planar PAH coronene across a range of temperatures relevant to combustion. The enhanced interactions between cPAHs and potassium ions resulted in significant and rapid nucleation of stable clusters compared to all other systems, highlighting their importance in soot nucleation. In addition, the resulting cPAH clusters present morphologies distinct from the stacked planar PAH clusters.

1 Introduction

Incomplete combustion produces carbonaceous particulate matter, known as soot, that negatively impacts combustion devices, human health and the environment (Benajes et al., 2015; Highwood and Kinnersley, 2006). The formation of soot particles is a complex chemical and physical process that involves gas phase chemistry of reactive precursor species and subsequent particle processes. The transition between gas phase molecules to solid particles is the least well understood aspect of soot formation. Proposed physical nucleation mechanisms suggest that dimerisation of polycyclic aromatic hydrocarbons (PAHs) plays a pivotal role, but the reversibility of this process, the high concentration of PAHs required, and the weak intermolecular interactions at high temperatures present difficulties (Eaves et al., 2015; Wang, 2011; Chung and Violi, 2011). Similarly, posited chemical inception mechanisms, which suggest stabilisation of nucleating particles by the formation of aliphatic links between aromatic molecules, do not fully describe all of the observed systems since they require a significant amount of hydrogen radicals and the predicted nascent particles have a much lower C/H ratio than is found in flames (Wang, 2011).

Recently, we have proposed that interactions between curved PAHs (cPAHs) and ions may play a significant role in soot formation (Martin, Bowal, Menon, Slavchov, Akroyd, Mosbach and Kraft, 2018; Martin, Botero, Slavchov, Bowal, Akroyd, Mosbach and Kraft, 2018). Curved aromatics, which differ from their planar counterparts through the integration of non-hexagonal rings into their predominately hexagonal arrangement, are found to comprise a significant portion of young soot particles (Botero et al., 2016; Wang et al., 2017; Martin, Botero, Slavchov, Bowal, Akroyd, Mosbach and Kraft, 2018). This non-planar structure has been shown to produce significant polarity in otherwise non-polar molecules. For example, coronene and corannulene are both PAHs consisting of a single concentric arrangement of aromatic rings, although in contrast to the planar coronene molecule corannulene is curved due to a central pentagonal ring. Coronene is non-polar while corannulene has a dipole moment of 2.07 debye (Lovas et al., 2005), which is similar to that of water at 1.85 debye (Shostak et al., 1991) (although a better comparison is made with the local dipole moment at the pentagonal site of corannulene which is $\approx$1.63 debye

given our previous analysis (Martin et al., 2017)). This charge polarisation is primarily due to the strain-induced shift of the electron density from the concave to convex side of the curved molecule, known as the flexoelectric effect (Martin et al., 2017). Experimental and computational work has determined that a representative nucleating soot molecule contains 15 rings, two of which are pentagons, and has a dipole moment of 5.32 debye (Martin, Botero, Slavchov, Bowal, Akroyd, Mosbach and Kraft, 2018).

The unique electrical properties of curved aromatics allow them to interact strongly with ions, which has been recently explored for its potential in supramolecular and materials chemistry applications (Filatov and Petrukhina, 2010; Zabula et al., 2018). Density functional theory (DFT) calculations have shown that the binding energy between a typical curved soot molecule and the chemi-ion $C_3H_3^+$ is 150–170 kJ/mol, suggesting that these interactions are strong enough to stabilise a small cluster of 1–1.5 nm at flame nucleating temperatures (1300–1500 K) (Martin, Botero, Slavchov, Bowal, Akroyd, Mosbach and Kraft, 2018; Glassman, 1989). Experimental evidence showing increased physical clustering with cations also supports an ionic mechanism of soot particle formation (Carbone et al., 2018, 2017). Ion-dipole, dipole-dipole, and dipole-induced-dipole interactions between cPAHs and ions are long-ranged, with the former scaling with the reciprocal of the separation distance squared, and the other two as the inverse separation cubed and to the sixth power respectively. These long-range interactions are likely to be especially significant in combustion systems where species are present in low concentrations. Our previous work has provided insight into these molecules and their interactions using electron microscopy and electronic structure calculations (Martin, Botero, Slavchov, Bowal, Akroyd, Mosbach and Kraft, 2018), but it remains unknown what effect these enhanced interactions have in a large system containing many cPAHs and ions. In order to develop more detailed understanding of the role of cPAHs and ions in the formation and structure of nascent soot particles, the simulation of dynamic systems is required to investigate the temperature dependent behaviour of cPAHs and ions and the morphology of resulting nanoparticles.

Molecular dynamics uses classical mechanics to study the movement and behaviour of molecular systems over time and provides valuable information about molecular interactions and ar-

rangements of nascent soot particles (Totton et al., 2012; Chen et al., 2014*b*,*a*; Iavarone et al., 2016; Grančič et al., 2016; Chung and Violi, 2011; Elvati and Violi, 2013; Bowal et al., 2018). These simulations require an accurate description of the interactions between constituent components, typically provided by an atom-atom potential in which the interaction energy at each point in time is calculated as a sum of pairwise interactions between atoms. An isotropic PAH potential (isoPAHAP) was developed using high accuracy intermolecular interaction energies from symmetry-adapted perturbation theory based on density functional theory (SAPT(DFT)) (Misquitta et al., 2005; Hesselmann et al., 2005; Podeszwa and Szalewicz, 2008) to provide an accurate description of intermolecular interactions of PAHs (Totton et al., 2010, 2012). This potential was an improvement from previous general hydrocarbon potentials, such as the Lennard-Jones (van de Waal, 1983) and Williams' (Williams, 1999, 2001) (W99) potentials, particularly at the T-shaped dimer geometries (Totton et al., 2010; Pascazio et al., 2017).

The isoPAHAP potential uses atom-centred, molecule-specific point charge models derived from a transferable distributed multipole model involving both charges and quadrupoles to describe the electrostatic properties of PAHs (Totton et al., 2011). This atom-centred charge-only representation is suitable for moderately sized planar PAH molecules for which the electrostatic interaction dominantly arises from the terminal groups where it can be modelled using atom-centred charges. In such systems there are no substantial local dipole terms within the PAH and the contributions from the quadrupolar terms are relatively minor compared to the dispersion and exchange-repulsion contributions. Consequently this model has been used successfully in a number of studies of PAH systems (Chen et al., 2014*b*,*a*; Grančič et al., 2016; Pascazio et al., 2017; Bowal et al., 2018). However in cPAH molecules, strain at the carbon sites results in charge polarisation through the flexoelectric effect, and this leads to the formation of local dipole moments at the carbon atoms in the interior of the molecule. These dipole moments cannot be captured by the atom-centred charge models used in the isoPAHAP model. For example, the isoPAHAP charge model incorrectly models the electrostatic potential around the curved corannulene molecule, as shown in Figure 2a. The dipole moment is found to be 1.73 debye, significantly reduced from the calculated and experimentally determined values of 2.07 debye (Martin et al., 2017).

An improved description of the electrostatic potential is provided by the distributed multipole expansion, which describes the charge distribution of a molecule using atom-centred multipole functions (Stone et al., 1985; Stone, 2005), but this is computationally expensive to use and not widely implemented in molecular dynamics software. In order to examine systems containing curved aromatics, a new potential needs to be developed that describes the flexoelectric effects in a computationally efficient and readily usable implementation.

This work aims to study the role of cPAHs and ions in stabilising nascent soot particles by investigating their clustering behaviour using an accurate intermolecular potential. In Section 2 an intermolecular potential (curPAHIP) is developed that is able to capture the flexoelectric effect and enhanced interactions of cPAHs and ions. Simple interaction energies for the small cPAH corannulene are compared with *ab initio* calculations. In Section 3, the curPAHIP potential is used within molecular dynamics simulations to provide information on homogeneous and ion-induced heterogeneous nucleation of corannulene, in comparison to analogous systems containing the planar coronene molecule. Clustering behaviour and resulting morphologies are explored across a range of temperatures relevant to soot formation. These results provide insight into how the interactions between cPAHs and ions affect the formation and structure of soot nanoparticles and provide valuable information towards expanding current soot models.

2 Developing a potential for curved PAHs

2.1 Determining the electrostatic potential

The isotropic all-atom isoPAHAP potential is used as the foundation for developing a potential able to describe curved PAHs. The isoPAHAP potential takes the following form,

$$U_{ab} = K \exp\left[-\alpha_{ab}\left(R_{ab} - \rho_{ab}\right)\right] - \left[1 - \exp\left(-\beta R_{ab}\right) \sum_{k=0}^{6} \frac{\left(\beta R_{ab}\right)^k}{k!}\right] \frac{C_{6,ab}}{R_{ab}^6} + \frac{q_a q_b}{R_{ab}}, \quad (1)$$

where the first term is the short-range term in the Born–Mayer form, the second term is the dispersion term damped by the Tang-Toennies damping function (Tang and Toennies, 1984), and

the third is the point charge electrostatic term. U denotes the interaction energy, K sets the energy unit of this term and will be taken to be 0.001 hartree in this work, α is the hardness parameter in the Born–Mayer term, R_{ab} is the atom-atom separation where a and b denote atomic sites within a molecule, ρ_{ab} is a shape parameter, β is the damping coefficient, $C_{6,ab}$ is a dispersion coefficient, and q is the atomic point charge. Further details about the parametrisation and form of the isoPAHAP potential can be found in Totton et al. (2010).

In this work the cPAH corannulene ($C_{20}H_{10}$), consisting of five hexagonal rings surrounding a pentagonal ring, is used as a representative cPAH. Although it is likely too small to contribute significantly to soot nucleation at flame temperatures (Martin, Botero, Slavchov, Bowal, Akroyd, Mosbach and Kraft, 2018), it provides a good starting point for the development of a cPAH potential with a distinct benefit of having been studied in previous *ab initio* studies. To incorporate the charge distribution created by curving a PAH, off-site point charges are added to the molecule description in a method similar to the multiple site models of water (Bernal and Fowler, 1933; Jorgensen et al., 1983). These mass-less virtual sites are fixed at a distance of 0.047 nm directly above each of the pentagonal carbons on the convex surface of the cPAH, as seen in Figure 1. This distance and the corresponding point charge values, found in Appendix A, were optimised to match DFT calculations which provide a good description of the electric potential around corannulene (Martin et al., 2017). This was done using the MULFIT programme, which fits atomic charges through a systematic reduction of the distributed multipole expansion (Ferenczy et al., n.d.).

[Figure 1 about here.]

This modified molecule description allows the dipole moment of corannulene to increase from 1.73 debye (using fitted atom-centred charges (Martin et al., 2017)) to a value of 2.14 D, in reasonable agreement ($< 4\%$ difference) with the known dipole moment of corannulene. Figure 2b shows that the electrostatic potential around corannulene after including the off-site point charge description is in good agreement with DFT results.

[Figure 2 about here.]

The use of the OPLS-AA forcefield for the intramolecular forces produces a geometry in good agreement to the corannulene structure determined by X-ray crystallography (Petrukhina et al., 2005) and DFT calculations (Martin et al., 2017). Corannulene is known to invert at room temperature (Scott et al., 1992), however molecules are considered rigid in these simulations since an inversion would require a coupling of the atomic charges with the geometry change. This inversion barrier rapidly increases as rings are added and therefore this model is appropriate for studying the interaction of ions and large curved arenes, which are observed in the flame (Martin, Botero, Slavchov, Bowal, Akroyd, Mosbach and Kraft, 2018).

2.2 Dimer binding energies

The binding energy of a corannulene dimer was assessed as a function of the dimer separation distance using several potential descriptions and the results are shown in Figure 3. The bowl-to-bowl "sandwich" configuration was considered since this is likely to be a low energy dimer configuration and SAPT(DFT) interaction energies are available (Cabaleiro-Lago et al., 2018). All evaluations of the intermolecular potentials were performed using the ORIENT programme (Stone et al., 2017).

From Figure 3 we see that the interaction energy is significantly underestimated using the isoPAHAP potential. Some disagreement could be expected because, as we have discussed above, the atom-centred charges used in the isoPAHAP potential underestimate the flexoelectric effect. However changing the electrostatic model in the isoPAHAP potential to a full multipole model derived specifically for corannulene or adding off-site charges do not cause a significant improvement in the interaction energies and the error remains large at the energy minimum separation. This is because the presence of pentagonal rings increases the dispersion interaction of the molecule by about 20%. This increase is known to occur for curved carbon nanostructures (Gobre and Tkatchenko, 2013).

[Figure 3 about here.]

We have addressed this difference through a re-optimisation of the relevant isoPAHAP pa-

rameters, specifically the dispersion coefficients ($C_{6,ab}$) and shape function (ρ_{ab}), to result in the curPAHIP model. The parameters were simultaneously refitted using SAPT(DFT) energies, which were weighted as in Totton et al. (2010) in order to favour more negative energies and thus ensure an accurate potential well. Harmonic constraints were used to prevent the parameters of curPAHIP from deviating too far from the corresponding isoPAHAP values. The resulting parameters are shown in Table 2 (SI units provided in Appendix A), and provide a weighted root mean square residual energy of 1.30 kJ/mol. Following Misquitta and Stone (2008) the dispersion damping term β is not fitted but is defined through the molecular vertical ionisation energy I as $\beta = 2(2I)^{1/2}$. Using the value of I for corannulene (Schröder et al., 2001), we obtain $\beta = 1.50$ a.u.

[Table 1 about here.]

As can be seen in Figure 3, the curPAHIP potential is able to capture the interaction behaviour of corannulene using off-site point charges and optimised dispersion parameters.

2.3 K^+ binding energies

SAPT(DFT) results of corannulene dimers show that induction energy, defined as the attractive energy due to the electron density of a molecule distorting in response to the electric field of another nearby molecule, is a very small component of the interaction, contributing to only 4% of the attractive energy (Cabaleiro-Lago et al., 2018). The curPAHIP potential, like isoPAHAP, does not model the induction energy (a combination of the classical polarisation and charge-transfer energies) as separate term, but instead absorbs the effects of the second-order induction into the dispersion and exchange-repulsion parameters. This is reasonable when the induction energy is a relatively small component of the total interaction energy, as it is in the interactions of both planar and curved PAH molecules. However the induction plays a significant role when ion interactions are involved, with energy contributions equal to or greater than those from the electrostatic component (Tsuzuki et al., 2001; Marshall et al., 2009; Schyman and Jorgensen, 2013). Incorporating a physical term that includes dynamic polarisation and charge-transfer into

atomic models comes at a very high computational cost due to the need for local coordinate systems for each atomic multipole, iterative solving of mutually induced dipoles, and the increased complexity of intra- and intermolecular terms. Instead it is sometimes possible to include polarisation effects indirectly within non-polarisable potentials with fixed charges by computing a set of polarised point charges obtained by treating the surrounding molecules in an average manner, typically via the introduction of a dielectric with suitable dielectric constant. Models obtained in this manner can be expected to be limited in that they are only applicable to the system they are designed for and the effective charge model is valid only for large-scale homogeneous systems.

A similar strategy was employed here and an effective interaction model was developed for a system containing potassium ions, K^+, and corannulene molecules. An effective charge model may not be appropriate for a heterogeneous system such as this since the molecular environment, and thus the polarisation, is not fixed but varies in space. Therefore we have developed an effective interaction model by altering the exchange-repulsion and dispersion terms in a Lennard-Jones potential form. This was done in a fitting procedure initialised from the OPLS-AA parameters for K^+ (Jensen and Jorgensen, 2006). Ensuring accurate binding energies was prioritised and so the K^+ parameters were fit to the maximum binding energy of corannulene and K^+ determined from hybrid DFT with an empirical dispersion correction (B97D/cc-pVTZ), which has been found to accurately describe binding energies of Na^+-benzene interaction to within 1.3 kJ/mol compared with CCSD(T)/CBS calculations (Neves et al., 2011). The resulting parameters, $\sigma = 9.64$ and $\epsilon = 3.43 \times 10^{-8}$ a.u. (SI units provided in Appendix A), provide an interaction energy of -87.7 kJ/mol. This agrees well with the binding energy of -88 kJ/mol determined from B97D. However the model results in a reduced equilibrium separation distance of 0.25 nm compared to 0.29 nm from DFT calculations. The underestimation of the separation provided by this fit is considered acceptable for the work discussed here since its potential consequences, such as increasing steric effects and corannulene-corannulene repulsion within clusters, result in a conservative estimate of K^+-corannulene interactions and clustering.

3 Nucleation simulations

Molecular dynamics simulations were used to investigate the homogeneous and ion-induced heterogeneous nucleation of the small curved aromatic molecule corannulene ($C_{20}H_{10}$, 250 g/mol) and its planar counterpart coronene ($C_{24}H_{12}$, 300 g/mol). The clustering behaviour and resulting morphologies were explored over a range of flame relevant temperatures. As the smallest curved PAH, corannulene is often used as a model molecule for fullerene-like species (Biase and Sarkisov, 2013). Thus its molecular properties, such as boiling and melting points, are established and it provides a useful system for assessing the behaviour of cPAHs in flames. Corannulene has been found to be present in flames (Lafleur et al., 1993), however its clustering effectiveness is expected to be less significant than those for larger curved molecules prevalent in sooting environments due to its weaker interaction energy. Potassium is readily ionised in a flame and has been shown to impact soot nucleation through the production of higher particle numbers and smaller particle sizes (Haynes et al., 1979; Di Stasio et al., 2011; Simonsson et al., 2017). Due to this known influence and the straightforward incorporation of the spherical potassium cation within an atomic model, K^+ provides a representative cation useful for exploring the interactions of cPAHs and ions in a large dynamic system. This system thus presents an exploratory study comparing the interactions of small curved and planar PAHs with and without cations.

3.1 Molecular dynamics methods

Molecular dynamics simulations were performed using the software GROMACS 5.1.4 (Abraham et al., 2015) according to a similar methodology detailed in our previous work (Totton et al., 2012). One thousand PAH molecules (coronene or corannulene) with and without the same number of potassium ions were randomly placed in a periodic box. This ratio and large number of molecules ensured proper statistics of molecular interactions and cluster stability. A concentration of 2×10^{18} cm^{-3} allowed experimentally relevant processes to be observed in the simulation timescale, as described in Totton et al. (2012). A two-step minimisation process using the steepest descent and low-memory Broyden-Fletcher-Goldfarb-Shanno approaches removed any

excess energy caused by the initial arrangement. Canonical simulations, defined by maintaining a constant number of atoms, system volume, and temperature, were then conducted for 1 ns with a timestep of 1 fs using a velocity Verlet integrator. A chain of 10 Nosé-Hoover thermostats was used for temperature control and intermolecular cut-offs were set to 3.0 nm. Electrostatic interactions were calculated at long range using particle-mesh Ewald summation. Intramolecular forces were determined using the OPLS-AA force field for molecule bonds, angles, dihedral and improper dihedral angles (Kaminski et al., 2001). The isoPAHAP potential was used to describe the coronene interactions while the newly developed curPAHIP intermolecular potential was used to describe corannulene interactions and enhanced Lennard-Jones parameters defined the interactions between K^+ and corannulene.

The clustering behaviour and resulting morphologies were explored at 500, 750, 1000, and 1500 K. Clusters were identified using a previous methodology that was shown to provide a suitable measure of stable clusters for PAHs ranging from 4 to 19 rings in size (Totton et al., 2012). This means that PAH molecules must be within 1.2 nm of each other for at least 20 ps to be considered bound in a cluster. Collision efficiencies and lifetimes were calculated to provide an assessment of nucleation propensity and stability of formed clusters. It is important to note that in this analysis a cluster must contain at least two PAHs, i.e. a single PAH interacting with an ion is not considered to be a cluster. Finally, cluster sizes and morphologies were also discussed.

3.2 Clustering over time

Figure 4 shows the extent of clustering for each system over time. The degree of clustering decreases with increasing temperature such that for all systems clusters are formed at 500 K but no lasting clusters are formed at 1500 K. At 500, 750, and 1000 K the coronene, coronene with K^+, and corannulene systems all experience a similar extent of clustering. This similarity between homogeneous corannulene and coronene systems is unsurprising since they have very similar binding energies (-65.7 kJ/mol for a coronene dimer (Podeszwa, 2010) and -65.9 kJ/mol for a corannulene dimer (Cabaleiro-Lago et al., 2018)). The clustering propensity of coronene

molecules is unaffected by the inclusion of cations in the system, in agreement with electronic structure calculations that suggest the π-cation interactions are not strong enough to impact clustering of planar PAHs (Chen and Wang, 2017).

In contrast, corannulene molecules with K^+ ions experience significantly more clustering than all other systems, with an increase of about 50% above the other systems at 500 K, 95% above at 750 K, and 92% above at 1000 K. The degree of corannulene clustering with K^+ is in fact very similar to that of the much larger ovalene molecule ($C_{32}H_{14}$, 398 g/mol) in a homogeneous system (Totton et al., 2012). Of particular interest is the fact that this enhanced clustering occurs to a significant degree even at 750 and 1000 K, which is above the sublimation point of corannulene at 640 K (Chickos et al., 2002). The number of clusters formed as a function of the simulation time (not shown) shows the same trends as those seen when examining the percentage of molecules clustered over time, indicating that the increase in clustering is primarily due to the formation of new clusters instead of cluster growth.

[Figure 4 about here.]

3.3 Collision efficiency

Further cluster statistics were evaluated to understand how these ion-cPAH interactions are able to increase the amount of clustering seen. Collision efficiency is defined as the number of successful collisions over the total number of collisions and thus indicates the "stickiness" of the interacting components.

Collision efficiencies for all the systems and temperatures studied in this work are shown in Figure 5a. Collision efficiencies decrease significantly with temperature since the increased kinetic energy serves to both increase the total number of collisions and decrease the ability for the molecules to bind strongly. The collision efficiency is the highest for corannulene molecules with K^+ ions, with a value above that observed for significantly larger planar PAHs (Totton et al., 2012). As seen in the degree of clustering over time, the inclusion of K^+ ions in the system containing coronene molecules has minimal effect on the cluster behaviour at all temperatures

studied. This is due to the weak bonding between the planar PAHs and cations and indicates that the ions do not act as seeds around which the clusters of planar PAHs form. In the simulation trajectories, we observe that few coronene molecules interact with the potassium ions even at 500 K, whereas a significant portion of corannulene molecules are bound to a cation at that temperature.

Interestingly the nature of the high collision efficiency for corannulene systems containing K^+ ions is not the same across all temperatures studied. Above 1000 K the total number of collisions is similar between all the systems and so this high efficiency comes from a significantly higher number of successful collisions. This highlights the importance of the ion-cPAH interaction in promoting nucleation at high temperatures. The inverse is true at 500 K: the number of successful collisions is relatively consistent across systems but the total number of collision events is more than 50% lower for corannulene with ions. This may be because clustering occurs more rapidly in the corannulene and K^+ system. Due to its larger mass, the average velocity of a cluster is lower than that of a single molecule at a given temperature, so an increase in the number of clusters reduces movement within the system and results in fewer collision opportunities. In addition, at low temperatures repulsive interactions between ions and polar cPAHs may play a significant role and prevent the short-lived cluster formation seen when weak dispersive interactions dominate the system. This is supported by the average cluster lifetimes reported in Figure 5b, discussed in more detail later. At 750 K the number of successful collisions is approximately 275% higher and the number of total collisions is about 30% lower for corannulene with K^+ compared to the other systems. These results show the ability of ions to promote clustering efficiency of cPAHs across a wide range of temperatures.

[Figure 5 about here.]

3.4 Cluster lifetimes

Cluster lifetimes show the stability of clusters after they are formed, which is crucial in the understanding of soot formation. Average cluster lifetimes, shown in Figure 5b, decrease with

temperature in all cases as expected. At low temperature (500 K), cluster lifetimes are long with some clusters lasting for nearly the entire simulation lifetime in all systems studied. At higher temperatures (750 K, 1000 K) the cluster lifetimes of corannulene molecules with K^+ ions are significantly higher than for other systems. At 1500 K, the average lifetimes of all systems studied are very low. Corannulene without ions exhibits slightly smaller cluster lifetimes compared to homogeneous coronene, as expected according to its molecular weight. However the average cluster lifetimes are much higher for corannulene with K^+ than for all the other systems, with an increase of up to 375%. These results show that at temperatures below 1500 K, the presence of the ion is significant in promoting long cluster stabilisation for corannulene molecules.

3.5 Cluster sizes and morphologies

Figure 5c shows the maximum cluster size obtained over the simulations studied. The maximum cluster sizes decrease as the simulation temperature increases such that only occasional dimers are formed at 1500 K. Despite significantly higher collision efficiencies for systems containing corannulene and K^+ ions compared to the other systems studied, their maximum cluster sizes are relatively similar. This indicates that for the simulation length considered here, the presence of ions has a more significant role in nucleation compared to cluster growth. Figure 6 provides snapshots of the maximum clusters formed at each temperature within the systems containing corannulene and K^+ ions.

[Figure 6 about here.]

The morphologies of clusters formed from cPAHs are significantly different than those made up of planar PAHs. Figure 7 shows cluster snapshots at 500 K for corannulene and coronene simulations with K^+ ions. These images indicate the typical and maximum cluster sizes over time and show observed cluster motifs.

[Figure 7 about here.]

Coronene molecules initially interact with K^+ ions in some cases although these interactions appear short lived and homogeneous clusters are more readily formed at 500 K. Homogeneous clusters primarily form single stacks, with some T-shaped interactions observed. Once a cluster grows to about four or five molecules, an ion is usually integrated into the structure. The planar PAHs cluster around the ion in a "propeller" motif, a staggered triangular arrangement which allows the cluster to be stabilised by cation-π and CH-π interactions. A maximum of three coronene molecules form the first solvation shell around the ion and dispersion interactions allow π-π stacking of further molecules.

In contrast to coronene, almost all corannulene dimers and clusters contain K^+ ions from very early in the simulation. The majority of K^+-corannulene interactions occur on the convex side of the curved molecule and only a few cases in which the K^+ interacts with the concave surface are observed. This is in agreement with DFT results, which found that the K^+-corannulene complex is more stable when the cation is on the convex surface compared to the concave side (Carrazana-García et al., 2011). The alignment of corannulene molecules around K^+ maximises electrostatic interactions. The first solvation shell around the ion consists of three or four molecules, with their convex surfaces pointing towards the ion, which we call a "flower" motif. This arrangement allows for further interactions with additional molecules, held together by a combination of dispersion and electrostatic interactions, to form shifted stacks extending out from the ion. Up to four corannulene molecules are able to bind strongly with a cation in contrast to the three molecules found for small planar PAHs (Chen and Wang, 2017).

An additional simulation of corannulene without K^+ ions was conducted for 10 ns at 500 K to provide a preliminary expected morphology of a large cluster of cPAHs for comparison with the known structure of large clusters of planar PAHs used in many previous molecular modelling studies investigating soot properties. Due to strong dispersive interactions, a tightly stacked structure is favoured for low energy clusters of planar PAHs, such as the coronene cluster containing 50 molecules shown in Figure 7 obtained from Chen et al. (2014*b*). In contrast, the large corannulene cluster shown here presents a more amorphous arrangement containing many disordered stacks containing 2–4 molecules. The cPAHs are often aligned with curved bowls slightly shifted

or arranged such that neighbouring molecules alternate in direction. These motifs are similar to those seen in studies examining the packing structure of solid state cPAHs (Filatov et al., 2010). π-π and electrostatic interactions promote the formation of small stacks, while the flexoelectric dipole enhances the CH-π interactions between the positively charged rim of one molecule and the negative π-surface of its neighbour which promote arrangements in which molecules are perpendicular to each other. The combination of these two interaction types serves to stabilise the three-dimensional structure of the corannulene cluster. This initial insight suggests that cPAHs promote a spherical cluster arrangement more similar to the concentric-ringed structure observed in microscopy images of soot (Alfè et al., 2009) but further work needs to be done to characterise the structure of cPAH clusters.

4 Discussion

No significant clusters were formed at 1500 K, indicating that even with stronger ion-cPAH interactions compared to planar PAHs, corannulene cannot contribute substantially to soot particle nucleation at flame temperatures. However, corannulene molecules did cluster around cations above their melting point, which suggests that the interactions between cPAHs and ions promote the nucleation process at high temperatures. We expect that this effect will be increased with larger cPAHs and smaller chemi-ions. Larger cPAHs have stronger electrostatic and dispersion interactions due to their larger dipole moment and molecule size, and this may provide sufficient additional binding energy to stabilise a cluster at flame temperatures. In addition, the binding energy between a corannulene molecule and K^+ ion is weaker than with a smaller cation due to a decrease in induction, a larger distribution of charge over the ion, and steric repulsion, particularly between the concave surface and large K^+ ion (Marshall et al., 2009). This is especially significant because for small cations the binding energy is greater between the cation and the concave surface of a cPAH compared to the convex surface, and this effect increases as the size of the cPAH increases (Carrazana-García et al., 2011). The fact that a small cation binds very readily to the concave surface of a larger cPAH is supported by the high interaction en-

ergy (-170 kJ/mol) of a 15-ringed cPAH with $C_3H_3^+$ (Martin, Botero, Slavchov, Bowal, Akroyd, Mosbach and Kraft, 2018). This arrangement would perhaps result in a nucleus structure which more closely resembles the experimentally observed seeds of primary soot particles from which an onion-like structure forms. We are currently exploring the interactions of larger cPAHs using the techniques developed here.

The models used in this study are based on accurate *ab inito* data, but they have important shortcomings: first, the present version of the curPAHIP potential does not take into account the increased polarisation of the cPAHs in proximity with the cation. This could be accounted for using an explicitly polarisable model, but while such models can be developed, and indeed have been for smaller organic molecules (Misquitta and Stone, 2016), we did not pursue this development in this study due to the increased computational cost of polarisable models. Second, while the cation-cPAH model that we have used is reasonable, the use of DFT as the reference and the too-short minimum configuration obtained with the model both lead to uncertainties; in particular, the latter error would lead to an increased steric repulsion between the cPAHs directly interacting with the cation. It is quite possible that a more advanced model, and one more carefully fitted to accurate *ab initio* data, will lead to more binding in systems such as those studied here.

Nevertheless, this work clearly illustrates the importance of considering the enhanced interactions present in curved carbon systems and provides insight into how the interactions between curved carbon molecules and ions affect the formation and structure of particulates in flames. Curvature has also been observed in many carbon structures such as glassy carbon, activated carbon and carbon blacks (Harris et al., 2008; Harris, 2004; Terzyk et al., 2012) and it is anticipated that the curPAHIP potential will be a valuable tool for describing the flexoelectric effect present in materials relevant to many other applications such as gas storage, separations, and microelectronics.

5 Conclusions

Curved PAHs containing five-membered rings are present in many carbon materials, including soot. Modelling the interactions between these molecules presents a challenge due to the flexoelectric dipole moment and enhanced dispersion interactions caused by the curvature. A new potential, curPAHIP, was developed using the foundations of the previously developed isoPAHAP potential. In this potential, the increased polarity of the cPAH is addressed with a modified molecule description in which off-site point charges are added to the pentagonal carbon atoms. This method was shown to properly describe the electrostatic potential and flexoelectric dipole moment of the small cPAH corannulene. The dispersion and shape function potential parameters were re-optimised to match SAPT(DFT) energies and enhanced parameters were determined to include polarisation with K^+ ion interactions.

We have demonstrated the value of the curPAHIP potential by applying it to a system relevant to soot formation. The clustering behaviour of corannulene molecules with and without K^+ ions was investigated using molecular dynamics and compared to analogous systems of the planar coronene molecule from 500–1500 K. In comparing PAHs with similar sizes and symmetry, we were able to highlight the effects of curvature and cations in the nucleation of PAHs. The clustering behaviours of coronene, coronene with K^+, and corannulene systems are very similar for all properties examined. In comparison, enhanced interactions between the polar corannulene molecules and K^+ ions result in more rapid and abundant clustering, higher collision efficiencies, and longer cluster lifetimes. The morphologies of corannulene clusters present a concentric arrangement in which bowl-to-bowl and T-shaped interactions are stabilised by dispersive and electrostatic interactions. This is different than the highly stacked structure of planar PAHs and perhaps more representative of experimentally observed soot particle structure. This work extends the current understanding of the role of planar and curved PAHs and ions in soot particle formation and provides an intermolecular potential valuable for the study of systems containing curved carbon.

Acknowledgments

This work used the ARCHER UK National Supercomputing Service (http://www.archer.ac.uk). K.B. is grateful to the Cambridge Trust and the Stanley Studentship at King's College, Cambridge for their financial support. This project is also supported by the National Research Foundation (NRF), Prime Minister's Office, Singapore under its Campus for Research Excellence and Technological Enterprise (CREATE) programme.

References

Abraham, M. J., Murtola, T., Schulz, R., Páll, S., Smith, J. C., Hess, B. and Lindah, E. (2015), 'GROMACS: High performance molecular simulations through multi-level parallelism from laptops to supercomputers', *SoftwareX* **1-2**, 19–25.

Alfè, M., Apicella, B., Barbella, R., Rouzaud, J. N., Tregrossi, A. and Ciajolo, A. (2009), 'Structure-property relationship in nanostructures of young and mature soot in premixed flames', *Proceedings of the Combustion Institute* **32 I**, 697–704.

Benajes, J., Martín, J., García, A., Villalta, D. and Warey, A. (2015), 'In-cylinder soot radiation heat transfer in direct-injection diesel engines', *Energy Conversion and Management* **106**, 414–427.

Bernal, J. D. and Fowler, R. H. (1933), 'A theory of water and ionic solution, with particular reference to hydrogen and hydroxyl ions', *The Journal of Chemical Physics* **1**(8), 515–548.

Biase, E. D. and Sarkisov, L. (2013), 'Systematic development of predictive molecular models of high surface area activated carbons for adsorption applications', *Carbon* **64**, 262 – 280.

Botero, M. L., Chen, D., González-Calera, S., Jefferson, D. and Kraft, M. (2016), 'HRTEM evaluation of soot particles produced by the non-premixed combustion of liquid fuels', *Carbon* **96**, 459–473.

Bowal, K., Martin, J. W. and Kraft, M. (2018), 'Partitioning of polycyclic aromatic hydrocarbons in heterogeneous clusters', *Carbon* .

Cabaleiro-Lago, E. M., Fernández, B. and Rodríguez-Otero, J. (2018), 'Dissecting the concave-convex π-π interaction in corannulene and sumanene dimers: SAPT(DFT) analysis and performance of DFT dispersion-corrected methods', *Journal of Computational Chemistry* **39**(2), 93–104.

Carbone, F., Canagaratna, M. R., Lambe, A. T., Jayne, J. T., Worsnop, D. R. and Gomez, A. (2018), 'Exploratory analysis of a sooting premixed flame via on-line high resolution (APi–TOF) mass spectrometry', *Proceedings of the Combustion Institute* .

Carbone, F., Moslih, S. and Gomez, A. (2017), 'Probing gas-to-particle transition in a moderately sooting atmospheric pressure ethylene/air laminar premixed flame. Part II: Molecular clusters and nascent soot particle size distributions', *Combustion and Flame* **181**, 329–341.

Carrazana-García, J. A., Rodríguez-Otero, J. and Cabaleiro-Lago, E. M. (2011), 'DFT study of the interaction between alkaline cations and molecular bowls derived from fullerene', *Journal of Physical Chemistry B* **115**(12), 2774–2782.

Chen, D., Totton, T. S., Akroyd, J., Mosbach, S. and Kraft, M. (2014*a*), 'Phase change of polycyclic aromatic hydrocarbon clusters by mass addition', *Carbon* **77**, 25–35.

Chen, D., Totton, T. S., Akroyd, J., Mosbach, S. and Kraft, M. (2014*b*), 'Size-dependent melting of polycyclic aromatic hydrocarbon nano-clusters: A molecular dynamics study', *Carbon* **67**, 79–91.

Chen, D. and Wang, H. (2017), 'Cation-π interactions between rlame chemi-ions and aromatic compounds', *Energy & Fuels* **31**(3), 2345–2352.

Chickos, J. S., Webb, P., Nichols, G., Kiyobayashi, T., Cheng, P.-C. and Scott, L. (2002), 'The enthalpy of vaporization and sublimation of corannulene, coronene, and perylene at T= 298.15 K', *The Journal of Chemical Thermodynamics* **34**(8), 1195–1206.

Chung, S. H. and Violi, A. (2011), 'Peri-condensed aromatics with aliphatic chains as key intermediates for the nucleation of aromatic hydrocarbons', *Proceedings of the Combustion Institute* **33**(1), 693–700.

Di Stasio, S., Legarrec, J. L. and Mitchell, J. B. (2011), 'Synchrotron radiation studies of additives in combustion, II: Soot agglomerate microstructure change by alkali and alkaline-earth metal addition to a partially premixed flame', *Energy and Fuels* **25**(3), 916–925.

Eaves, N. A., Dworkin, S. B. and Thomson, M. J. (2015), 'The importance of reversibility in modeling soot nucleation and condensation processes', *Proceedings of the Combustion Institute* **35**(2), 1787–1794.

Elvati, P. and Violi, A. (2013), 'Thermodynamics of poly-aromatic hydrocarbon clustering and the effects of substituted aliphatic chains', *Proceedings of the Combustion Institute* **34**(1), 1837–1843.

Ferenczy, G., Reynolds, C., Winn, P. and Stone, A. (n.d.), 'MULFIT: a program for calculating electrostatic potential-fitted charges, 1998', *May be obtained by contacting AJ Stone, email address: ajs1@ cam. ac. uk* .

Filatov, A. S. and Petrukhina, M. A. (2010), 'Probing the binding sites and coordination limits of buckybowls in a solvent-free environment: Experimental and theoretical assessment', *Coordination Chemistry Reviews* **254**(17-18), 2234–2246.

Filatov, A. S., Scott, L. T. and Petrukhina, M. A. (2010), 'π-π interactions and solid state packing trends of polycyclic aromatic bowls in the indenocorannulene family: Predicting potentially useful bulk properties', *Crystal Growth and Design* **10**(10), 4607–4621.

Glassman, I. (1989), 'Soot formation in combustion processes', *Symposium (International) on Combustion* **22**(1), 295–311.

Gobre, V. V. and Tkatchenko, A. (2013), 'Scaling laws for van der Waals interactions in nanostructured materials', *Nature Communications* **4**, 2341.

Grančič, P., Martin, J. W., Chen, D., Mosbach, S. and Kraft, M. (2016), 'Can nascent soot particles burn from the inside?', *Carbon* **109**, 608–615.

Harris, P. J. F. (2004), 'Fullerene-related structure of commercial glassy carbons', *Philosophical Magazine* **84**(29), 3159–3167.

Harris, P. J. F., Liu, Z. and Suenaga, K. (2008), 'Imaging the atomic structure of activated carbon', *Journal of Physics Condensed Matter* **20**(36).

Haynes, B., Jander, H. and Wagner, H. G. (1979), The effect of metal additives on the formation of soot in premixed flames, *in* 'Symposium (international) on Combustion', Vol. 17, Elsevier, pp. 1365–1374.

Hesselmann, A., Jansen, G. and Schütz, M. (2005), 'Density-functional theory-symmetry-adapted intermolecular perturbation theory with density fitting: A new efficient method to study intermolecular interaction energies', *Journal of Chemical Physics* **122**, 014103.

Highwood, E. J. and Kinnersley, R. P. (2006), 'When smoke gets in our eyes: The multiple impacts of atmospheric black carbon on climate, air quality and health', *Environment International* **32**(4), 560–566.

Iavarone, S., Pascazio, L., Sirignano, M., De Candia, A., Fierro, A., de Arcangelis, L. and D'Anna, A. (2016), 'Molecular dynamics simulations of incipient carbonaceous nanoparticle formation at flame conditions', *Combustion Theory and Modelling* **7830**, 1–13.

Jensen, K. P. and Jorgensen, W. L. (2006), 'Halide, ammonium, and alkali metal ion parameters for modeling aqueous solutions', *Journal of Chemical Theory and Computation* **2**(6), 1499–1509.

Jorgensen, W. L., Chandrasekhar, J., Madura, J. D., Impey, R. W. and Klein, M. L. (1983), 'Comparison of simple potential functions for simulating liquid water', *The Journal of Chemical Physics* **79**(2), 926–935.

Kaminski, G. A., Friesner, R. A., Tirado-Rives, J. and Jorgensen, W. L. (2001), 'Evaluation and reparametrization of the OPLS-AA force field for proteins via comparison with accurate quantum chemical calculations on peptides', *The Journal of Physical Chemistry B* **105**(28), 6474–6487.

Lafleur, A. L., Howard, J. B., Marr, J. A. and Yadav, T. (1993), 'Proposed fullerene precursor corannulene identified in flames both in the presence and absence of fullerene production', *The Journal of Physical Chemistry* **97**(51), 13539–13543.

Lovas, F. J., McMahon, R. J., Grabow, J. U., Schnell, M., Mack, J., Scott, L. T. and Kuczkowski, R. L. (2005), 'Interstellar chemistry: A strategy for detecting polycyclic aromatic hydrocarbons in space', *Journal of the American Chemical Society* **127**(12), 4345–4349.

Marshall, M. S., Steele, R. P., Thanthiriwatte, K. S. and Sherrill, C. D. (2009), 'Potential energy curves for cation-π interactions: Off-axis configurations are also attractive', *Journal of Physical Chemistry A* **113**(48), 13628–13632.

Martin, J. W., Botero, M., Slavchov, R. I., Bowal, K., Akroyd, J., Mosbach, S. and Kraft, M. (2018), 'Flexoelectricity and the formation of carbon nanoparticles in flames', *Journal of Physical Chemistry C* .

Martin, J. W., Bowal, K., Menon, A., Slavchov, R. I., Akroyd, J., Mosbach, S. and Kraft, M. (2018), 'Polar curved polycyclic aromatic hydrocarbons in soot formation', *Proceedings of the Combustion Institute* **18**, 1–7.

Martin, J. W., Slavchov, R. I., Yapp, E. K., Akroyd, J., Mosbach, S. and Kraft, M. (2017), 'The polarization of polycyclic aromatic hydrocarbons curved by pentagon incorporation: The role of the flexoelectric dipole', *Journal of Physical Chemistry C* **121**(48), 27154–27163.

Misquitta, A. J., Podeszwa, R., Jeziorski, B. and Szalewicz, K. (2005), 'Intermolecular potentials based on symmetry-adapted perturbation theory with dispersion energies from time-dependent density-functional theory', *Journal of Chemical Physics* **123**, 214103.

Misquitta, A. J. and Stone, A. J. (2008), 'Dispersion energies for small organic molecules: first row atoms', *Molecular Physics* **106**, 1631 – 1643.

Misquitta, A. J. and Stone, A. J. (2016), 'Ab initio atom-atom potentials using CamCASP: Theory and application to many-body models for the pyridine dimer', *Journal of Chemical Theory and Computation* **12**(9), 4184–4208. PMID: 27467814.

Neves, A. R., Fernandes, P. A. and Ramos, M. J. (2011), 'The accuracy of density functional

theory in the description of cation-π and π-hydrogen bond interactions', *Journal of Chemical Theory and Computation* **7**(7), 2059–2067.

Pascazio, L., Sirignano, M. and D'Anna, A. (2017), 'Simulating the morphology of clusters of polycyclic aromatic hydrocarbons: The influence of the intermolecular potential', *Combustion and Flame* **185**, 53–62.

Petrukhina, M. A., Andreini, K. W., Mack, J. and Scott, L. T. (2005), 'X-ray quality geometries of geodesic polyarenes from theoretical calculations: What levels of theory are reliable?', *Journal of Organic Chemistry* **70**(14), 5713–5716.

Podeszwa, R. (2010), 'Interactions of graphene sheets deduced from properties of polycyclic aromatic hydrocarbons', *Journal of Chemical Physics* **132**(4), 224704.

Podeszwa, R. and Szalewicz, K. (2008), 'Physical origins of interactions in dimers of polycyclic aromatic hydrocarbons', *Physical Chemistry Chemical Physics* **10**, 2735–2746.

Schröder, D., Loos, J., Schwarz, H., Thissen, R., Preda, D. V., Scott, L. T., Caraiman, D., Frach, M. V. and Böhme, D. K. (2001), 'Single and double ionization of corannulene and coronene', *Helvetica Chimica Acta* **84**(6), 1625–1634.

Schyman, P. and Jorgensen, W. L. (2013), 'Exploring adsorption of water and ions on carbon surfaces using a polarizable force field', *Journal of Physical Chemistry Letters* **4**(3), 468–474.

Scott, L. T., Hashemi, M. M. and Bratcher, M. S. (1992), 'Corannulene bowl-to-bowl inversion is rapid at room temperature', *American Chemical Society* (114), 1920–1921.

Shostak, S. L., Ebenstein, W. L. and Muenter, J. S. (1991), 'The dipole moment of water. I. Dipole moments and hyperfine properties of H_2O and HDO in the ground and excited vibrational states', *The Journal of Chemical Physics* **94**(9), 5875.

Simonsson, J., Olofsson, N. E., Bladh, H., Sanati, M. and Bengtsson, P. E. (2017), 'Influence of potassium and iron chloride on the early stages of soot formation studied using imaging LII/ELS and TEM techniques', *Proceedings of the Combustion Institute* **36**(1), 853–860.

Stone, A. J. (2005), 'Distributed multipole analysis: Stability for large basis sets', *Journal of Chemical Theory and Computation* **1**, 1128–1132.

Stone, A. J., Alderton, &. M. and Alderton, M. (1985), 'Distributed multipole analysis: Methods and applications', *Molecular Physics* **56**(5), 1047–1064.

Stone, A. J., Dullweber, A., Engkvist, O., Fraschini, E., Hodges, M. P., Meredith, A. W., Popelier, P. L. A. and Wales, D. J. (2017), 'ORIENT: a program for studying interactions between molecules, version 4.9'.

Tang, K. T. and Toennies, J. P. (1984), 'An improved simple model for the van der Waals potential based on universal damping functions for the dispersion coefficients', *The Journal of Chemical Physics* **80**, 3726–3741.

Terzyk, A. P., Furmaniak, S., Gauden, P. A., Harris, P. J. and Kowalczyk, P. (2012), *Virtual Porous Carbons*, Elsevier.

Totton, T. S., Misquitta, A. J. and Kraft, M. (2010), 'A first principles development of a general anisotropic potential for polycyclic aromatic hydrocarbons', *Journal of Chemical Theory and Computation* **6**(3), 683–695.

Totton, T. S., Misquitta, A. J. and Kraft, M. (2011), 'A transferable electrostatic model for intermolecular interactions between polycyclic aromatic hydrocarbons', *Chemical Physics Letters* **510**(1-3), 154–160.

Totton, T. S., Misquitta, A. J. and Kraft, M. (2012), 'A quantitative study of the clustering of polycyclic aromatic hydrocarbons at high temperatures', *Physical Chemistry Chemical Physics* **14**(14), 4081–4094.

Tsuzuki, S., Yoshida, M., Uchimaru, T. and Mikami, M. (2001), 'The origin of the cation/π interaction: The significant importance of the induction in Li^+ and Na^+ complexes', *The Journal of Physical Chemistry A* **105**(4), 769–773.

van de Waal, B. W. (1983), 'Calculated ground-state structures of 13-molecule clusters of carbon dioxide, methane, benzene, cyclohexane, and naphthalene', *The Journal of Chemical Physics* **79**(8), 3948.

Wang, C., Huddle, T., Huang, C. H., Zhu, W., Vander Wal, R. L., Lester, E. H. and Mathews, J. P. (2017), 'Improved quantification of curvature in high-resolution transmission electron microscopy lattice fringe micrographs of soots', *Carbon* **117**, 174–181.

Wang, H. (2011), 'Formation of nascent soot and other condensed-phase materials in flames', *Proceedings of the Combustion Institute* **33**(1), 41 – 67.

Williams, D. E. (1999), 'Improved intermolecular force field for crystalline hydrocarbons containing four- or three-coordinated carbon', *Journal of Molecular Structure* **485-486**, 321–347.

Williams, D. E. (2001), 'Improved intermolecular force field for molecules containing H, C, N, and O atoms, with applications to nucleoside and peptide crystals', *Journal of Computational Chemistry* **22**, 1154–1166.

Zabula, A. V., Spisak, S. N., Filatov, A. S., Rogachev, A. Y. and Petrukhina, M. A. (2018), 'Record alkali metal intercalation by highly charged corannulene', *Accounts of Chemical Research* **51**(6), 1541–1549.

A Supplementary Data

A.1 Corannulene geometry and charges

Corannulene elements, geometry (x, y, z in nm) and charges, in the curPAHIP potential. The element X represents the virtual mass-less atoms used to describe the flexoelectric effect, which are held above and parallel to the pentagon ring using intramolecular forces.

```
35
CORANNULENE with curPAHIP charges
C          0.103   0.064   0.085    0.020
C          0.093  -0.078   0.085    0.020
C         -0.045  -0.112   0.085    0.020
C         -0.121   0.008   0.085    0.020
C         -0.030   0.117   0.085    0.020
C          0.205   0.129   0.022    0.177
C          0.310   0.049  -0.032   -0.201
C          0.300  -0.090  -0.032   -0.201
C          0.187  -0.156   0.022    0.177
C          0.143  -0.279  -0.032   -0.201
C          0.007  -0.313  -0.033   -0.201
C         -0.090  -0.225   0.022    0.177
C         -0.242   0.016   0.022    0.177
C         -0.296  -0.103  -0.032   -0.201
C         -0.222  -0.222  -0.032   -0.201
C         -0.280   0.142  -0.031   -0.201
C         -0.190   0.250  -0.031   -0.201
C         -0.059   0.235   0.023    0.177
C          0.049   0.310  -0.032   -0.201
```

C	0.178	0.258	-0.032	-0.201
H	-0.221	0.345	-0.072	0.133
H	0.031	0.408	-0.072	0.133
H	0.259	0.317	-0.073	0.133
H	0.398	0.097	-0.072	0.133
H	0.380	-0.149	-0.075	0.133
H	0.215	-0.348	-0.073	0.133
H	-0.024	-0.408	-0.074	0.133
H	-0.265	-0.312	-0.073	0.133
H	-0.396	-0.103	-0.074	0.133
H	-0.378	0.155	-0.073	0.133
X	0.103	0.064	0.132	-0.063
X	0.093	-0.078	0.132	-0.063
X	-0.045	-0.113	0.132	-0.063
X	-0.121	0.008	0.133	-0.063
X	-0.030	0.117	0.133	-0.063

A.2 curPAHIP parameters in SI units

[Table 2 about here.]

A.3 K^+ interaction parameters in SI units

$\sigma = 0.51$ nm and $\epsilon = 0.00009$ kJ/mol

List of Figures

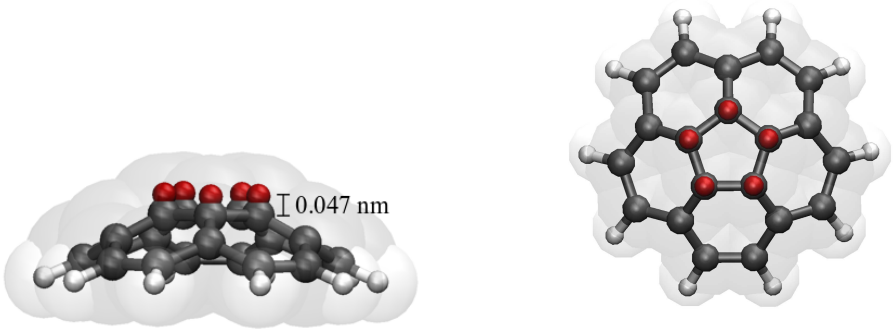

(a) *Side view* **(b)** *Top view*

Figure 1: *Geometry of the curved PAH corannulene ($C_{10}H_{20}$) with added off-site charges fixed above the pentagonal carbons. Carbon atoms are shown in grey, hydrogen atoms are shown in white, and off-site charges are shown in red.*

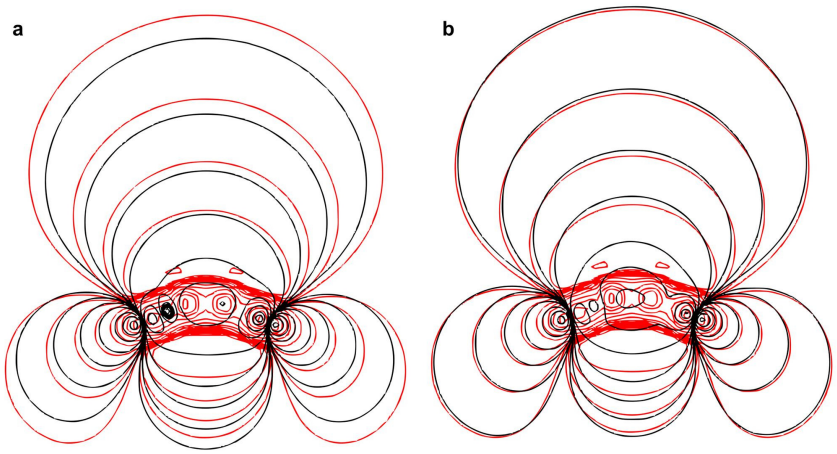

Figure 2: *Comparison of the electrostatic potential of corannulene calculated using DFT (red) and a potential description for implementation in molecular simulations (black). (a) shows the isoPAHAP potential using atom-centred charges. (b) shows the curPAHIP potential in which the electrostatic potential more closely matches the DFT results by using off-site charges.*

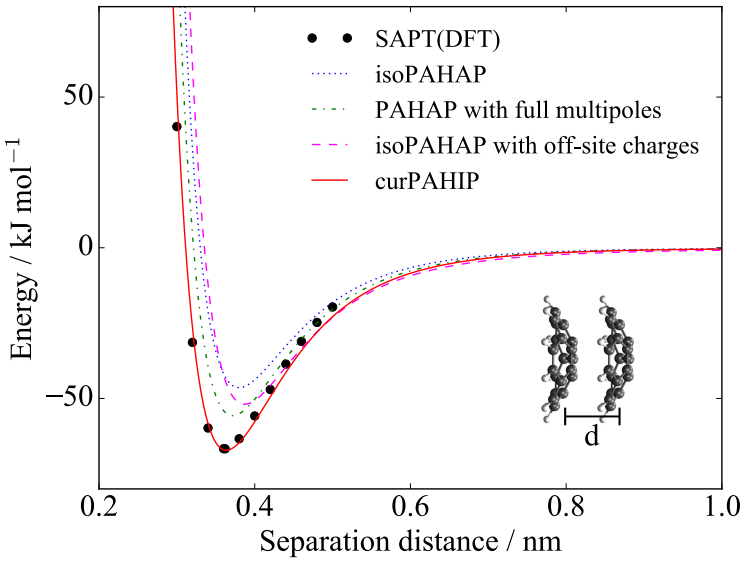

Figure 3: *Interaction energy versus separation distance for a corannulene dimer determined from SAPT(DFT) calculations (Cabaleiro-Lago et al., 2018), the isoPAHAP potential, the PAHAP potential with full multipoles, the isoPAHAP potential with off-site charges, and the isoPAHAP potential with off-site charges and re-fitted dispersion parameters (curPAHIP).*

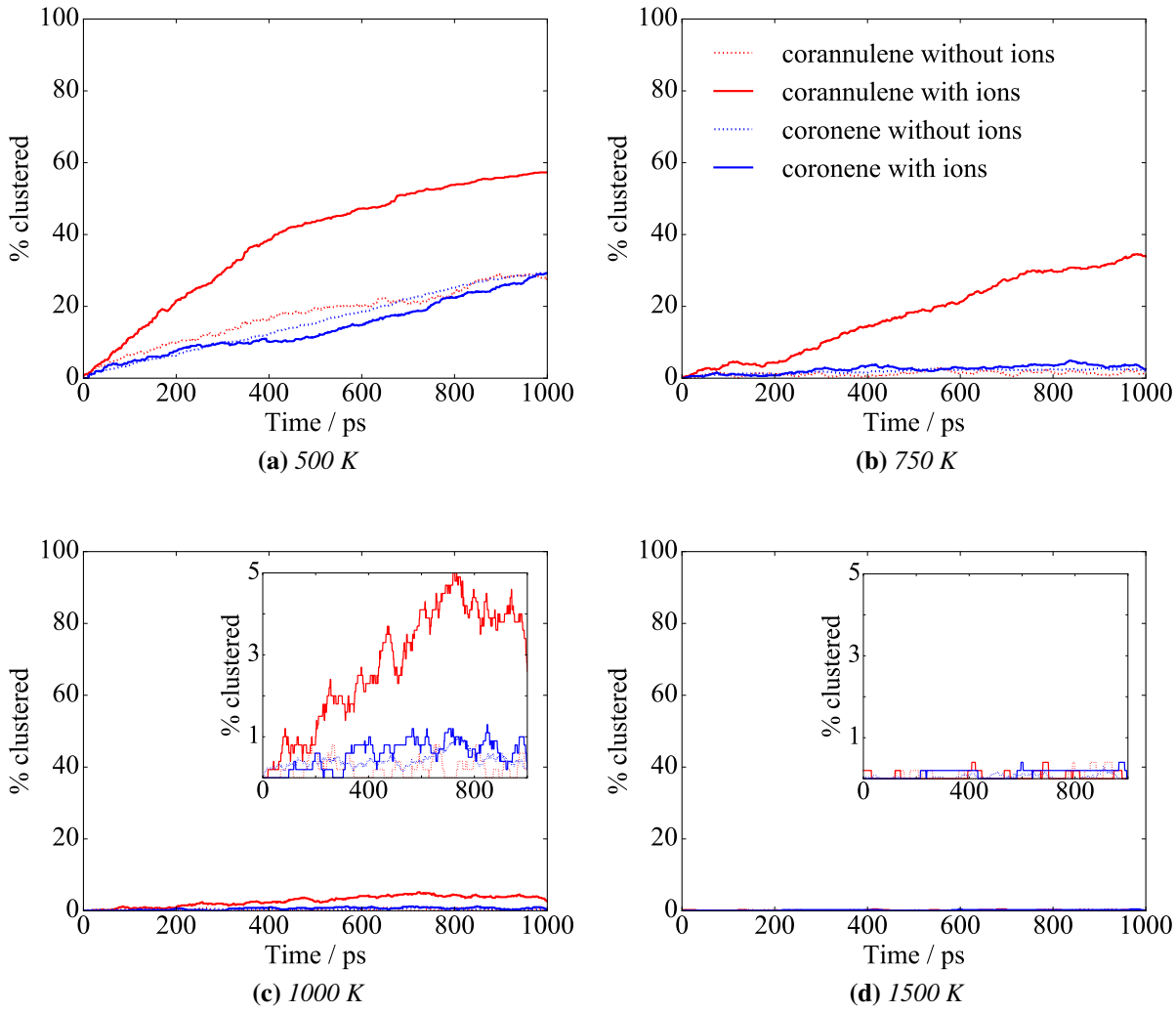

(a) *500 K* **(b)** *750 K*

(c) *1000 K* **(d)** *1500 K*

Figure 4: *Extent of molecules clustered over time for corannulene (red) and coronene (blue) systems at (a) 500 K, (b) 750 K, (c) 1000 K, and (d) 1500 K. Solid lines represent systems with potassium ions present and dashed lines indicate systems containing no potassium ions. Inset figures provide a closer look at the clustering trends at high temperatures.*

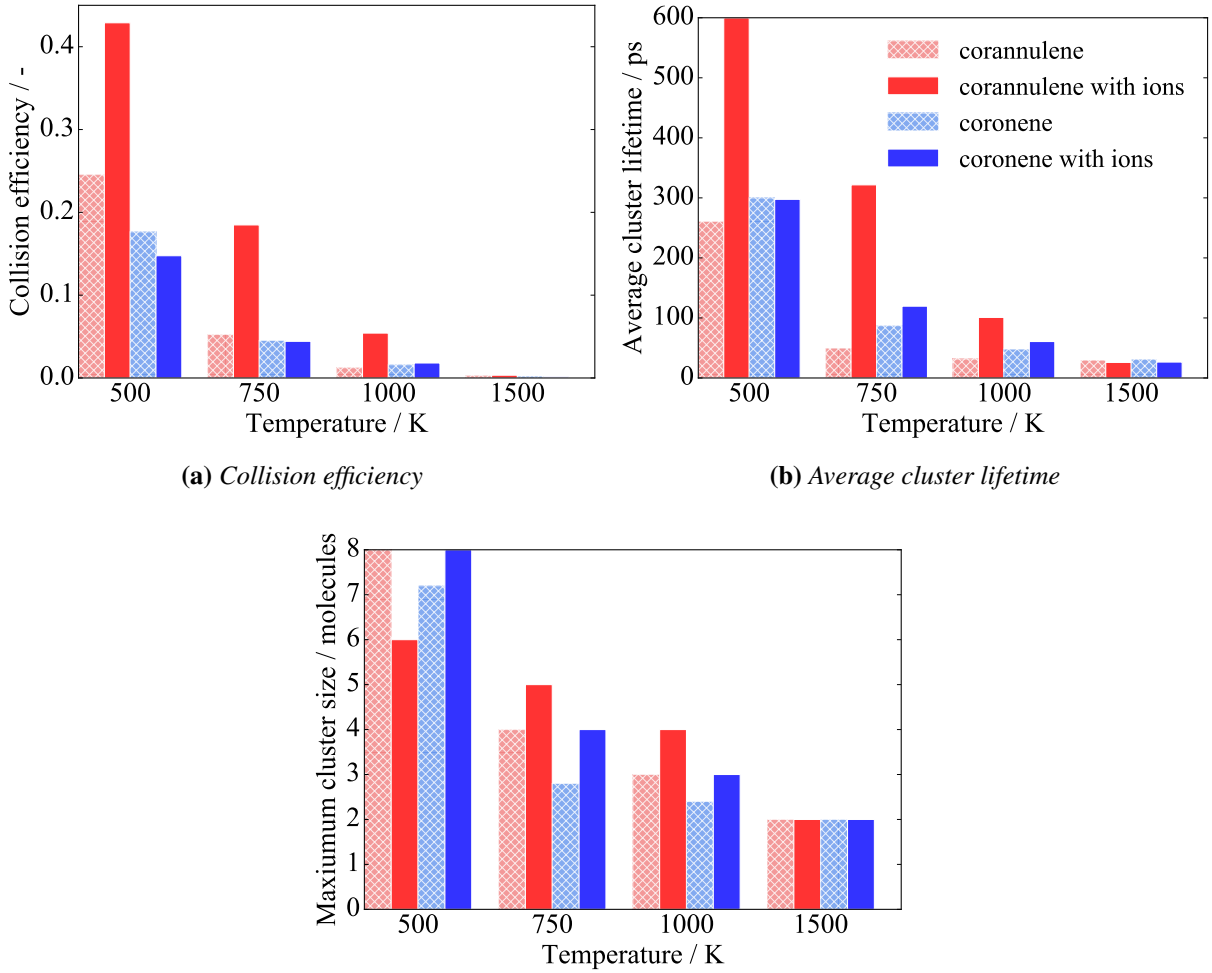

(a) *Collision efficiency*

(b) *Average cluster lifetime*

(c) *Maximum cluster size*

Figure 5: *Cluster properties over 1 ns simulations containing planar or curved PAHs with and without K^+ ions. (a) provides collision efficiencies, (b) reports average cluster lifetimes, and (c) presents maximum cluster sizes. Systems containing corannulene are shown in red, systems containing coronene are shown in blue, and the hatching indicates systems without K^+ ions present.*

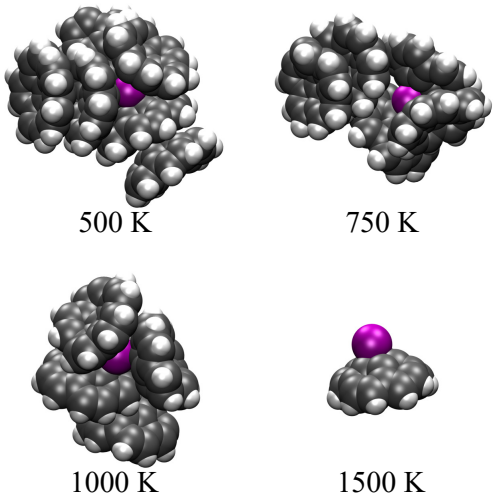

Figure 6: *Maximum clusters and complexes formed in simulations containing corannulene molecules and K^+ ions at 500, 750, 1000, and 1500 K. At the highest temperature (1500 K) dimers are rare and short-lived, so the more common and stable complex of K^+ and corannulene is shown here. Carbon atoms are shown in grey, hydrogen in white, and potassium in purple. Off-site virtual atoms are not shown.*

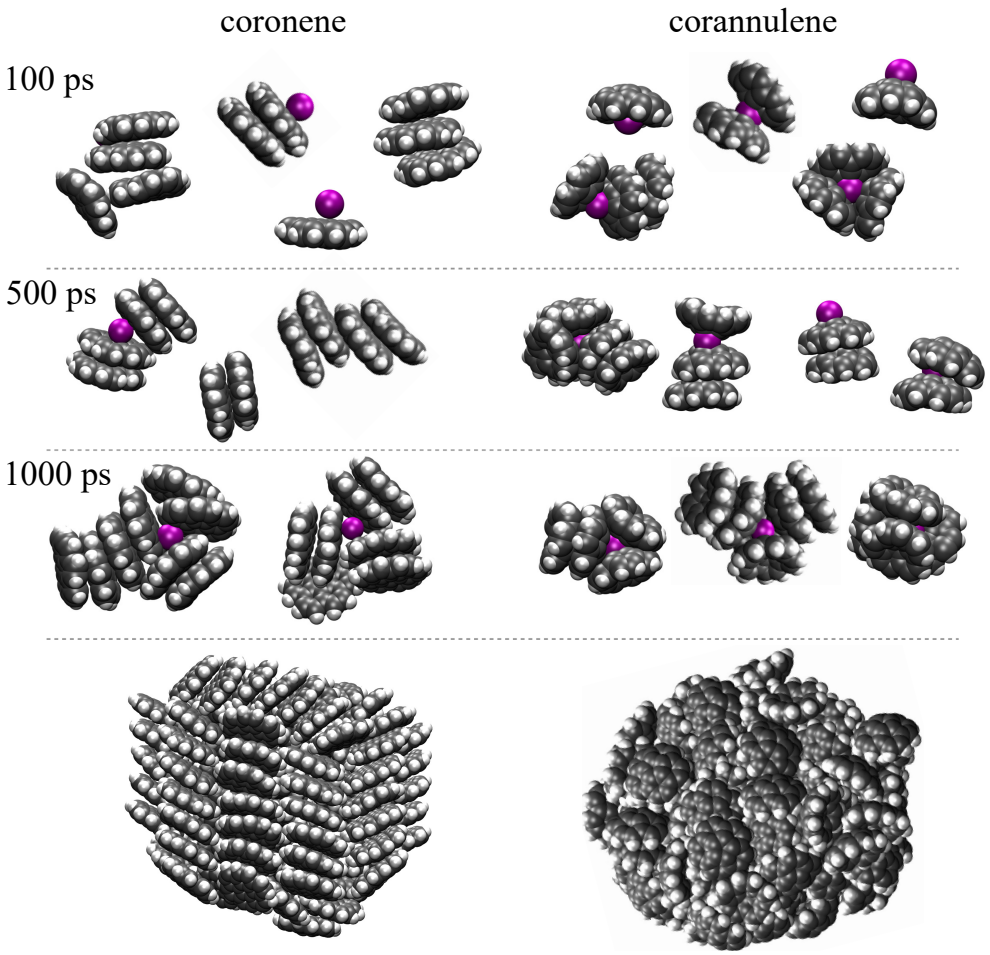

Figure 7: *Coronene and corannulene clusters formed at 500 K in the presence of K^+ ions at 100, 500, and 1000 ps. Expected arrangements of large clusters after an extended simulation without ions are shown for coronene (Chen et al., 2014b) and corannulene molecules (bottom). Carbon atoms are shown in grey, hydrogen in white, and potassium in purple. Off-site virtual atoms are not shown.*

List of Tables

Table 1: *Parameters of curPAHIP in a.u.*

Atom pair	ρ	α	C_6
C C	5.6563	1.8783	30.282
C H	4.9320	1.7560	12.604
H H	4.1187	1.4043	5.2179

Table 2: *Parameters of curPAHIP in SI units*

Atom pair	ρ (nm)	α (nm^{-1})	C_6 (kJmol^{-1}nm^6)
C C	0.2993	35.49	0.0017458
C H	0.2610	33.18	0.00072665
H H	0.2180	26.54	0.00030083